A study on fracture behavior of semi-elliptical 3D crack in claypolymer nanocomposites considering interfacial debonding

A Study on Fracture Behavior of Semi-Elliptical 3D Crack in Clay-Polymer Nanocomposites Considering Interfacial Debonding

Meghdad Zahedi[*,1], Reza Malekimoghadam[*,2,3], Roham Rafiee[3], Ugo Icardi[2]

[1] Department of Mechanical Engineering, Amirkabir University of Technology, Tehran, Iran

[2] Department of Mechanical and Aerospace Engineering, Polytechnic University of Turin, Turin, Italy

[3] Composites Research Laboratory, Faculty of New Sciences & Technologies, University of Tehran, End of The North Karegar St., Tehran 1439955941, Iran

Abstract

In the current research, the influence of clay platelet on crack characteristics of fully exfoliated clay/ polymer matrix is scrutinized. A multi-scale 3-D finite element model comprising of four phases as clay platelet, non-perfect bond interactions, interphase region and surrounding matrix is constructed to investigate semi-elliptical matrix crack properties, as a nano-notch, subjected to fracture mode I. Subsequently, the strain energy release rate is acquired in terms of J-integral parameter considering the location and dimension, geometrical variables and modeling strategy. The results imply on the pronounced effect of clay debonding on crack behavior which leads to local stiffness reduction. Furthermore, interphase characteristics such as thickness and elastic modulus, have significant influences on the critical energy release rate. The results are consistent with published literatures and the model can be invoked as a viable tool to investigate the fracture behaviors of clay/polymer nanocomposites.

Keywords: A. Nano-structures; B. Debonding; B. Fracture; C. Finite element analysis (FEA);

1. Introduction

Regarding the virtues of nanoparticle-reinforced polymeric composites, application of these materials pervades the state-of–the-art technologies in the aerospace, marine, automotive and other similar thriving industries. Owing to the superior mechanical, physical and thermal properties of polymeric nanocomposites with addition of carbon nanotube, nanoclay or

[*] Corresponding Author. *Email Address:* zahedi.m@aut.ac.ir
[*] Corresponding Author. *Email Address:* reza.malekimoghadam@polito.it , reza.malekimoghadam@gmail.com

nanoparticles, against pristine polymers, wide-range of investigations have been conducted in order to characterize of such materials [1-12]. Due to striking properties of nanoclay, the variation of elastic modulus and tensile strength pursuant to its content ratio in epoxy was vastly examined in some studies [13-17] considering various procedures. Among different clay types, Montmorillonite (MMT) is extensively exploited as nano-reinforcing agent in constructing nanocomposite materials due to its high aspect ratio and moderate cost [18]. A comprehensive review on nanoclay and nanoclay reinforced polymers, meanwhile, was accomplished by Rafiee and Shahzadi [19]. A profound investigation was carried out by Woong et al. [20] to identify the impact of clay dispersion on the mechanical properties and the results disclosed inevitable effect of material preparation process technique besides the amount of clay on fracture toughness and other attributes. In addition to elastic modulus, many experimental studies have been conducted in order to achieve fracture parameters including several matrix materials [21-24]. The effect of loading rates on fracture work and failure mechanism of polypropylene/nanoclay composite was expounded by Saminathan et al. [25, 26] in which the results demonstrated the measured fracture properties by the Essential Work of Fracture (EWF) method and dependency of fracture attributes on loading rate. Furthermore, their conclusions revealed that the specific EWF for yielding increased with the rise in the loading rate whilst the specific EWF for necking decreased. The increase in epoxy toughness after mixing both nanoclay and thermoplastic materials was reported by Rostamiyan et al. [27], in which, the obtained results indicated that the tensile, compressive and impact strength of the new ternary nanocomposites were ameliorated as opposed to those of neat resin. Considering debonding damage between interphase and nanoclay, the mechanical properties of nanoclay reinforced nanocomposite were acquired by Malekimoghdam et al. through finite element multi-scale modeling [28].

Notwithstanding the comprehensive experimental macro-scale clay/epoxy studies, a relatively infrequent number of researches could be found focused on the numerical 3D fracture behavior of nanocomposites in nano/micro scale. Furthermore, most researches put forward a 2D finite element representative volume element to investigate the mechanical behavior of exfoliated and intercalated clay-nanocomposites [29-31]. Silani et al. [32] conducted the experimental and numerical investigations in macro-scale exploring the effect of clay on the brittleness of the nanocomposite and damage initiation simulation in dog-bone sample by means of XEFM. Gaoming Dai et al. [33] elucidated damage behavior of nanoclay/polymers in a FEM analysis

employing disk-shape inclusion as nanoparticle reinforcing material without considering stress singularities by means of singular elements. It was observed that the rise in aspect ratio leads to an increase in Young's modulus, yet a decrease in strength. A semi- concurrent modeling approach on 2D fully exfoliated clay/ epoxy nanocomposite materials was utilized by Silani et al. [34] in order to find out the damage initiation and propagation through the material. Invoking phase field model, the fracture parameters of fully exfoliated clay/ polymer nanocomposites were obtained in some other literatures [35, 36].

Numerical studies regarding interactions of 2D cracked matrix in vicinity of a nanoparticle or nano fiber were presented in some literatures [37–40], in which the linear crack front interaction with carbon fibers or spherical inclusions were investigated without incorporating cohesive zone material model and debonding damage.

Considering the cumbersome procedure of performing experimental tests and the existing of limited computational investigations in this scope, the main aim of the present work is to propose a novel approach for studying the interaction between an epoxy matrix weakened by a semi-elliptical crack as a built-in nano-cleavage, and clay platelet via 3-D finite element method. For this purpose, a new Representative Volume Element (RVE) which is realistically capable of capturing clay debonding effect at nano/ micro scale is developed. The current study investigates the influence of clay on fracture behavior of cracked epoxy by conducting a comparative study between nanocomposite and neat resin. Unlike 2-D analysis and with the aid of semi-elliptical crack model, representing nonlinear crack front, the influence of interphase thickness on fracture behavior of RVE is also revealed.

2. Finite Element Modeling

There have been two mainstreams in developing numerous models that have been formed to assess nanocomposite mechanical properties [41–43], such models, namely two- and three-phase models, without and with considering the interphase between inclusion and surrounding matrix, respectively. In the present work, the investigated RVE consists four distinct phases as clay platelet, interface between clay and neighboring interphase (exerting cohesive zone model), clay/matrix interphase and epoxy matrix representing exfoliated morphology of nano-clay in matrix. A 3-D FE model of the RVE is built in ANSYS 15.0 commercial package. There are two approaches to construct RVE model representing different load transfer mechanisms from matrix

medium to inclusion, namely long type modeling and fully-embedded short clay modeling. It should be notified, long RVE approach is utilized to facilitate the simulation procedure and consequently some essential aspects of damage phenomenon are inevitably neglected. Given that, the nanoclay is extended throughout the whole length of RVE, in fact, normal debonding damage between nanoclay and interphase region is not captured because of inherent physics of long RVE model, while the interfacial interaction between them is simulated via cohesive zone model where only tangential deboning may occur. The "long type RVE" is selected by some researchers to evaluate nanoclay mechanical properties [43-45]. In this research, both 'Short RVE' and 'Long RVE' are analyzed to investigate the effect of clay length on the results. It is worthwhile to note that, in the 'Long RVE; the load is directly applied to the clay platelet, while, in the 'short RVE' the load transferring phenomenon from matrix to nano-clay is implemented by interphase and interphase phases. The constructed finite element models of both long and short types are illustrated in Fig.1.

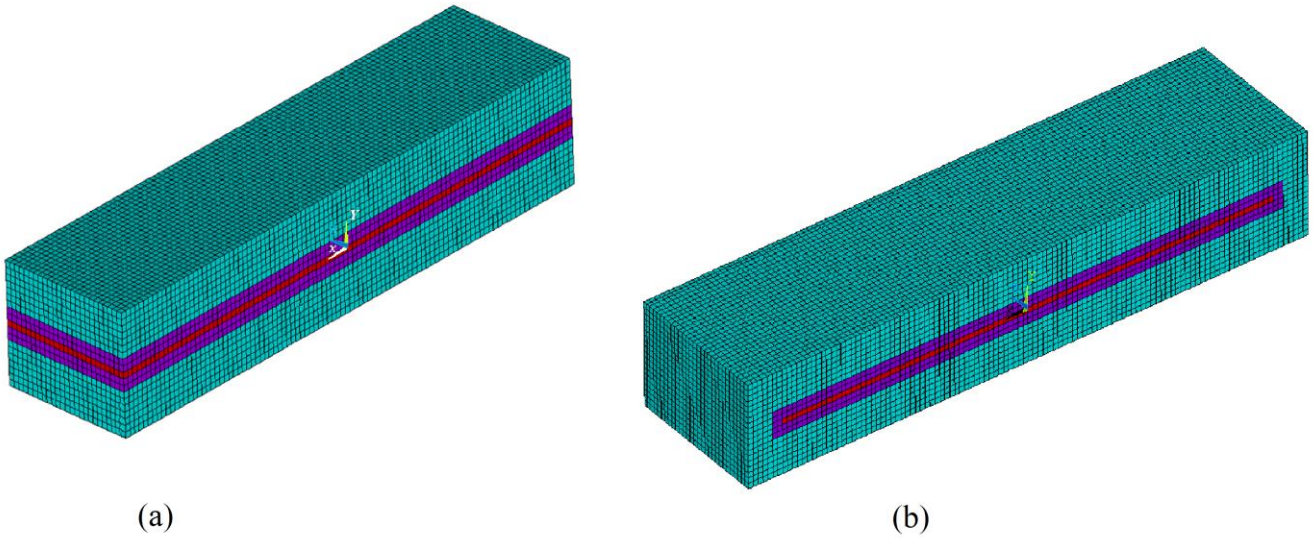

Fig. 1. Finite element model of intact half RVE (a) Long RVE (b) Short RVE

Regarding the 'Short RVE' model, it should be noted that the clay platelet is totally surrounded by polymer matrix and load transfer phenomenon is accomplished via non-bonded interphase region. Employing RVE with the aid of mixed-mode CZM, therefore, both normal and tangential clay debonding processes can be captured. The multi-scale finite element modeling procedure of four-phase intact nanocomposite is shown in Fig.2. It is worth mentioning that interphase is modeled as mobility region considering the variation of mechanical properties between matrix

and clay, while interface is invoked for the purpose of simulating interactions and debonding between clay and surrounding medium.

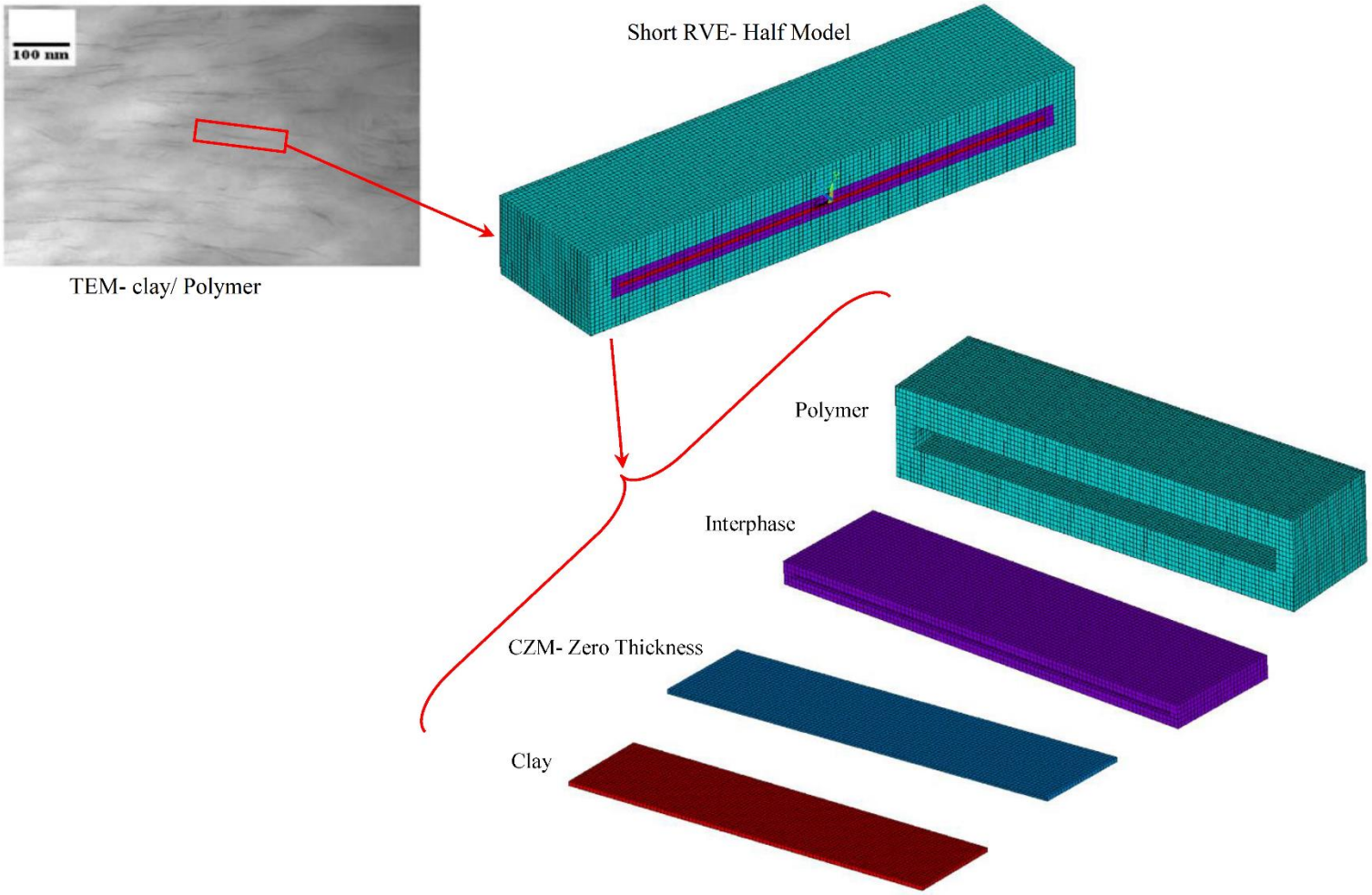

Fig. 2. Multi-scale finite element modeling procedure of four-phase clay/ polymer nanocomposite

2.1 Clay platelet

The clay platelet is simulated as an elastic isotropic material with the same material properties as Montmorillonite [46]. The thickness of each platelet is assumed to be 1nm [47]. The SOLID 186 element has been employed to construct the finite element of the clay model. This element possesses 20 nodes with three degrees of freedom per node which are transitional in x, y and z

directions [48]. Additionally, because of the usage of an intermediate node on each edge of the element, it has higher order shape function and thus results in a higher accuracy [48].

2.2 Surrounding Matrix

Considering various weight percentages of clay, the epoxy resin has been simulated with the SOLID 186 element. Epoxy mechanical properties are based on elastic-perfect-plastic material model derived from existing datasheets. The multi-linear isotropic hardening plasticity is adopted to simulate a finite element model which may be preferred for cycling where the kinematic hardening could exaggerate the Bauchinger effect [48]. Furthermore, a maximum of 100 stress-strain points can be defined to explain polymer behavior [48].

2.3 Interphase and Interface regions

The key issue defining the efficiency of improving the properties of clay/polymer nanocomposites at micro-scale is the load transferring phenomenon from the resin to the clay platelet through the interactions between the clay and the matrix occurring at interphase region. Thus, accounting for the load transferring mechanism from the matrix to the clay, modeling both interphase and interface (interactions between the clay and the matrix at interphase region) regions plays a crucial role in a proper understanding of the polymer clay nanocomposites (PCN). Consequently, the aforementioned region is divided into two segments comprising the mobility region and the interactions between epoxy and clay (at interphase region) which are simulated as the interphase and the interface (CZM model), respectively, according to Fig. 2.

2.3.1. Interphase region

Interphase, as an intermediate phase between clay and surrounding polymer, possesses dissimilar mechanical properties in comparison with clay and matrix properties. Modeling of this phase has a pivotal influence on the mechanical characteristics of both intercalated and exfoliated clay nanocomposites [49]. The interphase region between the surrounding matrix and the clay can exhibit as a mobility region [49] for which the mechanical properties vary from the clay to the matrix with different values reported for the thickness magnitude [45]. The elastic modulus of any point within clay/epoxy interphase, by introducing r as a parameter which varies within interphase thickness, can be specified by [43, 50]:

$$E_{int}(r) = E_m\left(\frac{l_{int}}{2r}\right) + [(l_{int} - 2r)/(l_{int} - l_c)]^{\frac{n}{2}}\left[E_c - E_m\left(\frac{l_{int}}{l_c}\right)\right] \quad (1)$$

Which is subjected to following constrains:

$$\begin{aligned} @r &= \frac{l_{int}}{2}, & E_{int} &= E_m \\ @r &= \frac{l_c}{2}, & E_{int} &= E_c \end{aligned} \quad (2)$$

where l_{int} is interphase length, l_c is clay length, E_m and E_c denote matrix and inclusion elastic modulus, respectively. The *n* denotes the Interfacial Enhancement Index (IEI) which depends upon the surface treatment of nanoparticles as well as the degree of intercalation/exfoliation occurring in nanocomposites; smaller magnitudes of IEI lead to higher interphase stiffness. By increasing the value of *n*, modulus function behavior will be akin to homographic functions. By virtue of mean value theorem for functions, the average of elastic modulus on interphase thickness can be found as follows.

$$\bar{E}_{int} = \frac{1}{th_{int}}\int_{l_c/2}^{l_{int}/2} E_{int}(r)dr \quad (3)$$

Fig.3 represents the interphase elastic modulus variation through its thickness. The magnitude of *n* which is ascribed to the interfacial facets of nanocomposite, can be found using single experimental tests. The effect of foregoing index on crack energetic is investigated in the following section.

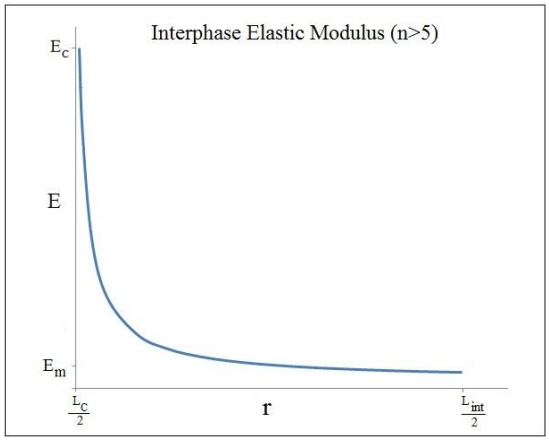

Fig. 3. Young modulus distribution versus interphase thickness

2.3.2. Interface Region

The interface region is introduced as a non-perfect bonding between clay and interphase and which is constructed via cohesive zone model. The zero thickness INTER204 3D element is employed to simulate interactions and debonding between clay and epoxy at interphase region. This model is a robust implement for simulating the interface debonding and related fracture phenomenon which is based on the model proposed by Alfano et al. [51]. This element is defined by 16 nodes having three degrees of freedom at each node in the x, y, z directions as shown in Fig. 4. Likewise, it is capable of simulating an interface between two surfaces and the subsequent delamination process, where the separation is represented by an increasing displacement between initially coincident nodes, within the interface element itself. Because the CZM encircles the entire clay platelet, the mixed-mode type including mode I and mode II is adopted to simulate interfacial debonding and fracture phenomena in both normal and tangential directions based on the bilinear traction-separation law. The CZM model consists of a constitutive relation between the traction "T" acting on the interface and the corresponding interfacial separation **"δ"** (displacement jump across the interface). The bilinear cohesive law is exploited under mixed-mode fracture in which the separation of material interfaces depends on both the normal and tangential components of displacement jumps which are displayed in Fig. 4. To take into account the difference in the normal and tangential jumps contributions to the separation of material interfaces, a non-dimensional effective displacement jump, λ for mixed-mode fracture is defined.

The normal and tangential components of cohesive tractions and corresponding relations in mixed-mode type are expressed as [48]:

$$T_n = K_n \delta_n (1-D_m) \tag{4}$$

$$T_t = K_t \delta_t (1-D_m) \tag{5}$$

$$\lambda = \sqrt{(\frac{\delta_n}{\delta_n^c})^2 + \beta^2 (\frac{\delta_t}{\delta_n^c})^2} \tag{6}$$

T_n, T_t, δ_n, δ_t, D_m describe normal traction, tangential traction, normal separation, tangential separation and damage parameter, respectively.

The β is the non-dimensional parameters which assigns different weights to tangential and normal displacement jumps. The damage parameter associated with mixed-mode bilinear cohesive law is illustrated as:

$$D_m = \begin{cases} 0 & \lambda_{max} = \lambda_\alpha \\ Min\ (1, dm) & \lambda_{max} > \lambda_\alpha \end{cases} \quad (7)$$

where:

$$\lambda_{cr} = \frac{\delta_n^*}{\delta_n^c} = \beta\frac{\delta_t^*}{\delta_t^c} \quad (8)$$

$$d_m = \eta\left[\frac{\lambda max - \lambda cr}{\lambda max}\right] \quad (9)$$

$$\eta = \frac{\delta_n^c}{\delta_n^c - \delta_n^*} = \frac{\delta_t^c}{\delta_t^c - \delta_t^*} \quad (10)$$

where δ_n^c / δ_t^c and δn^*/ δ_t^*, indicate normal/tangential displacement jump at the completion of debonding and normal/tangential displacement jump at maximum normal cohesive traction, respectively. There are six basic parameters to define the bilinear mixed-mode cohesive law in ANSYS [48] provided by the molecular dynamics simulation for the Van der Waals interactions between surfactants adhered to the clay surface and the surrounding matrix [49].

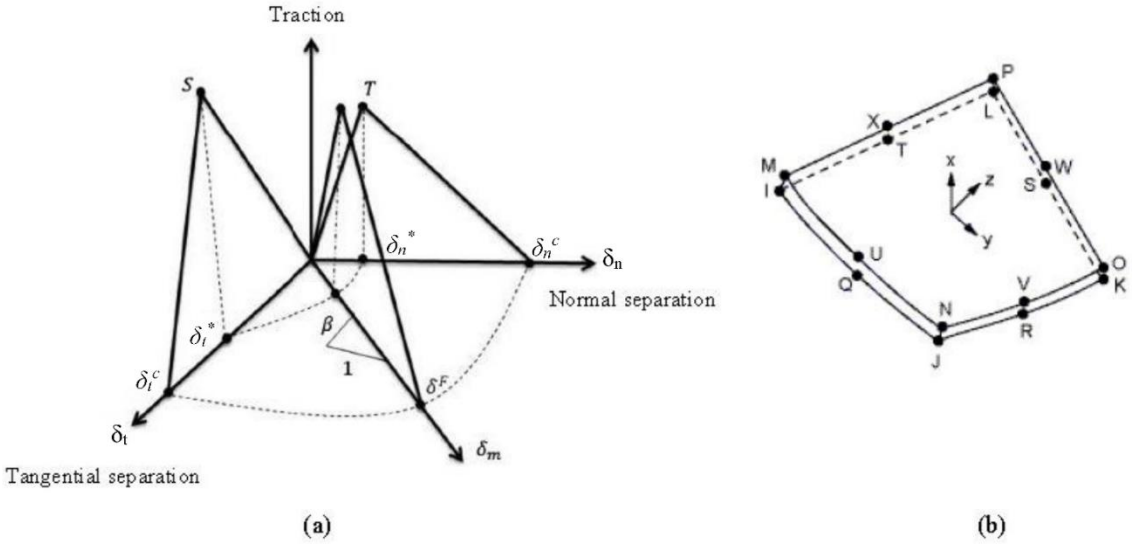

Fig. 4. Cohesive zone material (a) Mixed-mode traction-separation behavior (b) INTER204 element geometry [48]

2.4 Semi-elliptical 3D crack modeling

Generally speaking, stress and deformation fields around the crack tip have high gradients. The precise nature of these fields depends on the material, geometry, and other factors such as loading conditions. Additionally, convergence considerations would entail using higher order elements with higher order shape functions. As it can be seen in Figs. 5 and 6, in order to capture the rapidly varying stress and deformation fields, a refined mesh pattern is constructed in the region adjacent to crack front, utilizing hexahedral 20-node solid element (SOLID186). In these figures, crack location is indicated by x_c and RVE length, width and height are defined by l, w and $2t$, respectively.

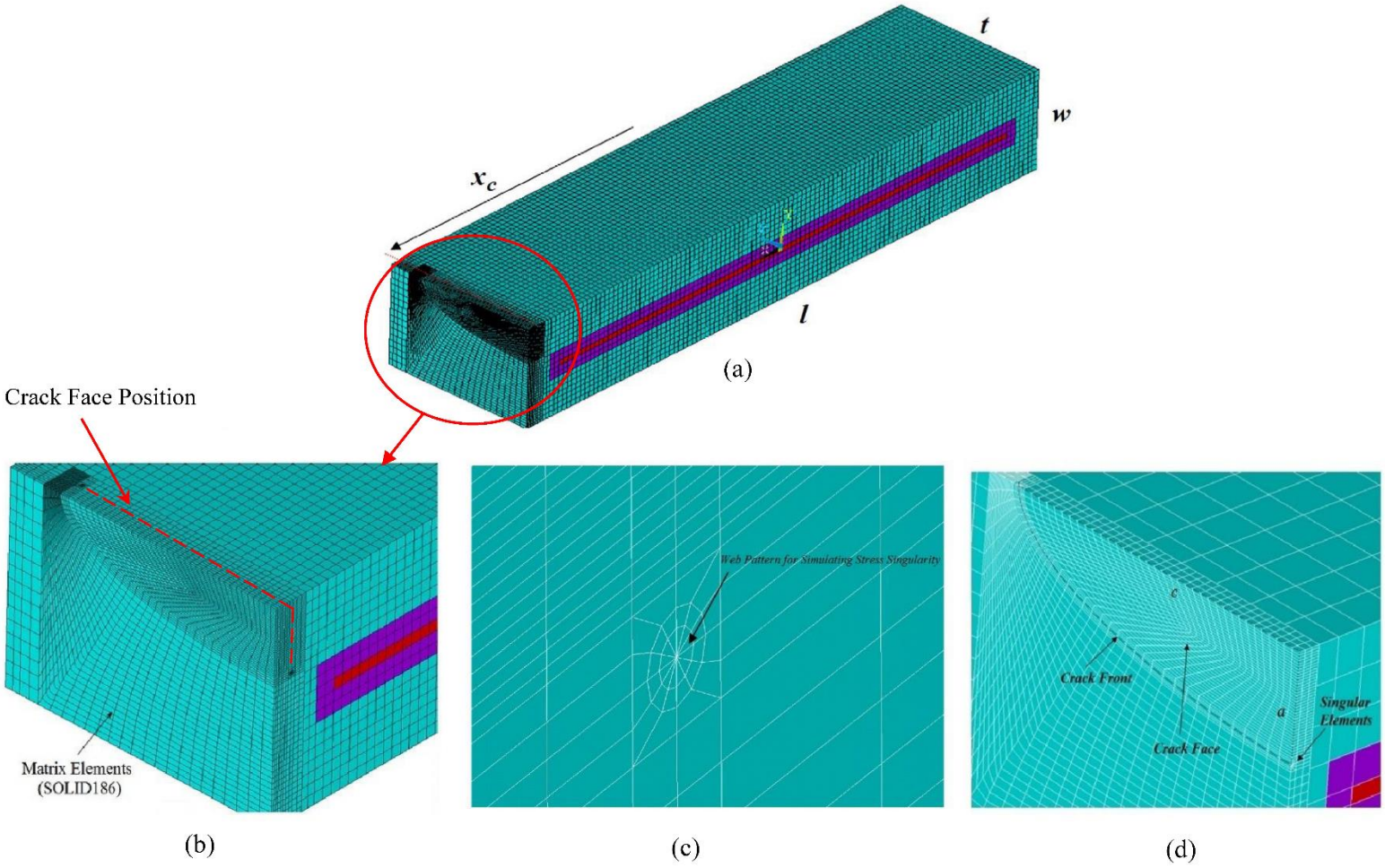

Fig. 5. (a) Finite Element model of short RVE with 3D crack (b) Enlarged view of crack face, (c) Spider web shape of singular elements (d) Cut- view at crack face/ crack parameters

Producing singularity in stress field, the crack front mesh (i.e. possessing elements next to the crack front) is chosen as a wedge-shape quadratic, with the mid-side nodes placed at the quarter point [52].

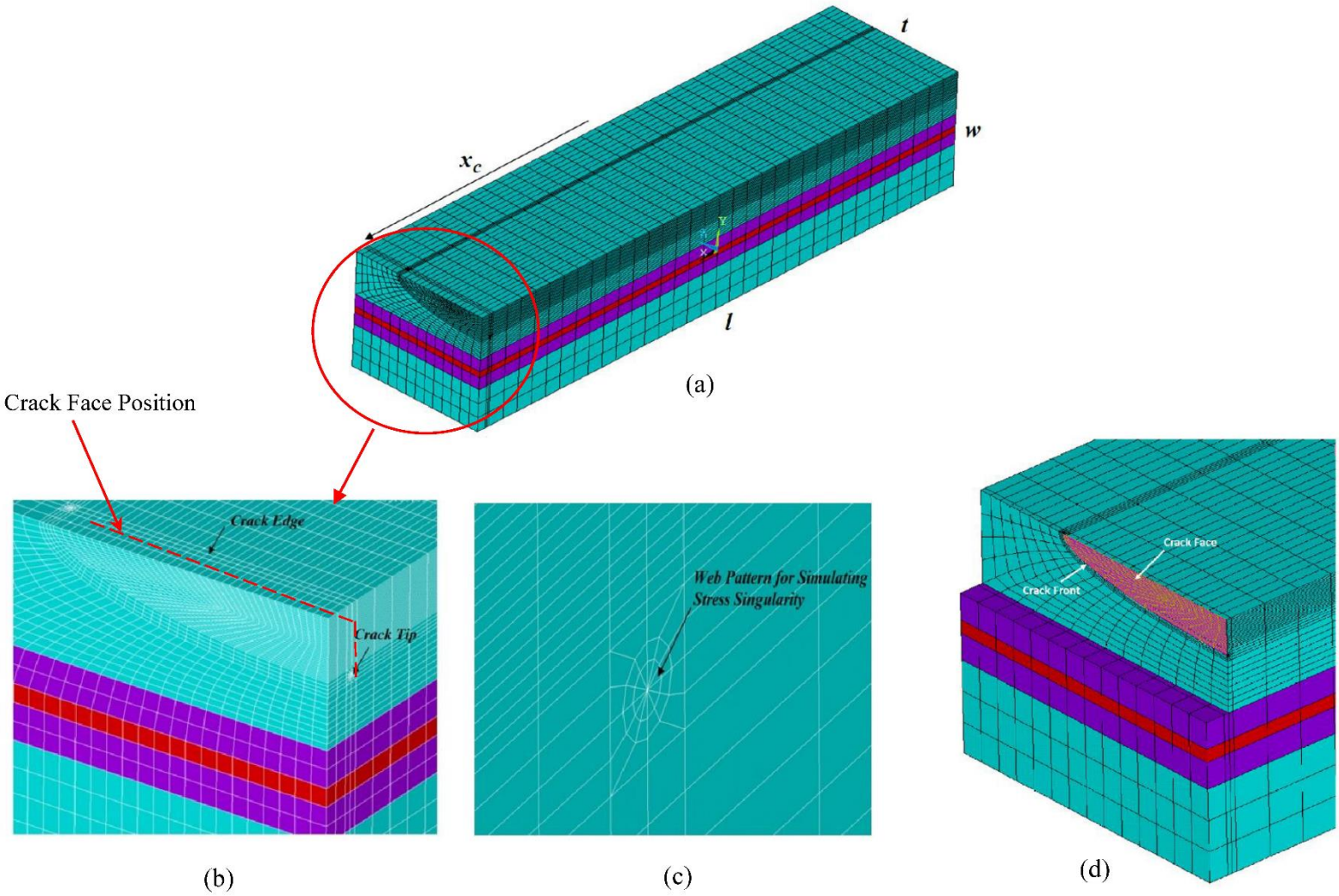

Fig. 6. (a) Finite Element model of Long RVE with 3D crack, (b) Enlarged view of crack structure, (c) Spider web shape of singular elements (d) Cut- view at crack face/ crack parameters

3. Results and Discussions

Prior to the elaboration of the outcomes, in order to verify the accuracy of the constructed FE model, a comparison is performed between the tensile stress-strain behavior of experimental study [53] and also finite element model [19] in the absence of any cracks. A very good agreement for the small strains (less than 2%) is observed signifying the RVE accuracy.

Regarding the loading process, a monotonic displacement in longitudinal direction was exerted to the end side of the model, while for the nodes belonging to the opposite side, the rotational and translational degrees of freedom are totally constrained.

Extracting proper mesh density in the crack front, a neat resin block is employed under pure tension with semi-circular crack (a=c) embedded in mid-plane section that is highly related to the typical closed form solution for mode I stress intensity factor given by [54]:

$$K_I = \frac{2}{\pi}\sigma\sqrt{\pi a} \tag{6}$$

where a is the crack radius and σ is the nominal remote tensile stress. In comparison with crack dimension, the resin block is large enough implying a valid analogy between infinite domain and aforesaid simulation. As a criterion for verifying the model, the computed stress intensity factor in finite element analysis based on contour-integral determination has deviation 1.2-1.6% from the exact values of above formulation showing reasonable accuracy. These results were attained by a crack front element size of c/50 where c stands for half of a crack's longer diameter [55, 56].

Due to the intrinsic non-linear behavior of CZM interaction, full Newton-Raphson iterative method was employed and the model was subjected to 1.5% of nominal strain.

As an energy-based criterion for determining the onset of crack growth, J-integral is implemented to specify energy release rate in the current model. The original form of the J-Integral for a line contour surrounding the crack tip(Γ) could be written as [57]:

$$J = \int_{\Gamma} \left(w dy - T_i \frac{\partial u_i}{\partial x} \right) ds \tag{7}$$

In which,

$$w = \int \sigma_{ij} d\varepsilon_{ij} \tag{8}$$

whereby w denotes the strain energy density ($\sigma_{ij}$and ε_{ij}as stress and strain tensor components),

$$T_i = \sigma_{ij} n_j \tag{9}$$

where T_i is the component of the traction vector which acts on the contour, u_i is the displacement component, and *ds* is a length increment along the contour Γ. Moreover, it should be noted that J- Integral is nothing but non-linear energy release rate defined by:

$$J = \frac{-d\Pi}{da} \tag{10}$$

where

$$\Pi = U - V \tag{11}$$

where, Π is the total potential energy. U and V stand for strain energy and external work, respectively. Pursuant to path-independency nature of J-integral and in the absence of any restrictions for plastic region size, this integral is an appropriate tool for assessing the fracture behavior based on numerical methods, hence, it is applied in the present work.

The total elastic-plastic strain contours of short and long RVE models are illustrated in Fig. 7 and 8, respectively. As expected, the maximum strain value is observed in the vicinity of deepest crack tip and in this case debonding damage phenomenon occurs at about 1.1% of strain. It is apparent from the contours supplied, in the short RVE that the total strain is greater than long RVE, since in the former the loading is transferred from matrix to clay via interphase, whereas in the latter, the load is directly imposed to clay platelet. Under longitudinal stress, strain concentration at the interphase-epoxy boundary also initiates after the detachment of clay along X direction due to the heterogeneous material properties of this region as delineated in Fig 7 (a), (b). The mentioned area is subjected to sharp elastic modulus variation and according to Hook's law, the magnitude of strain in this zone increases drastically [58].

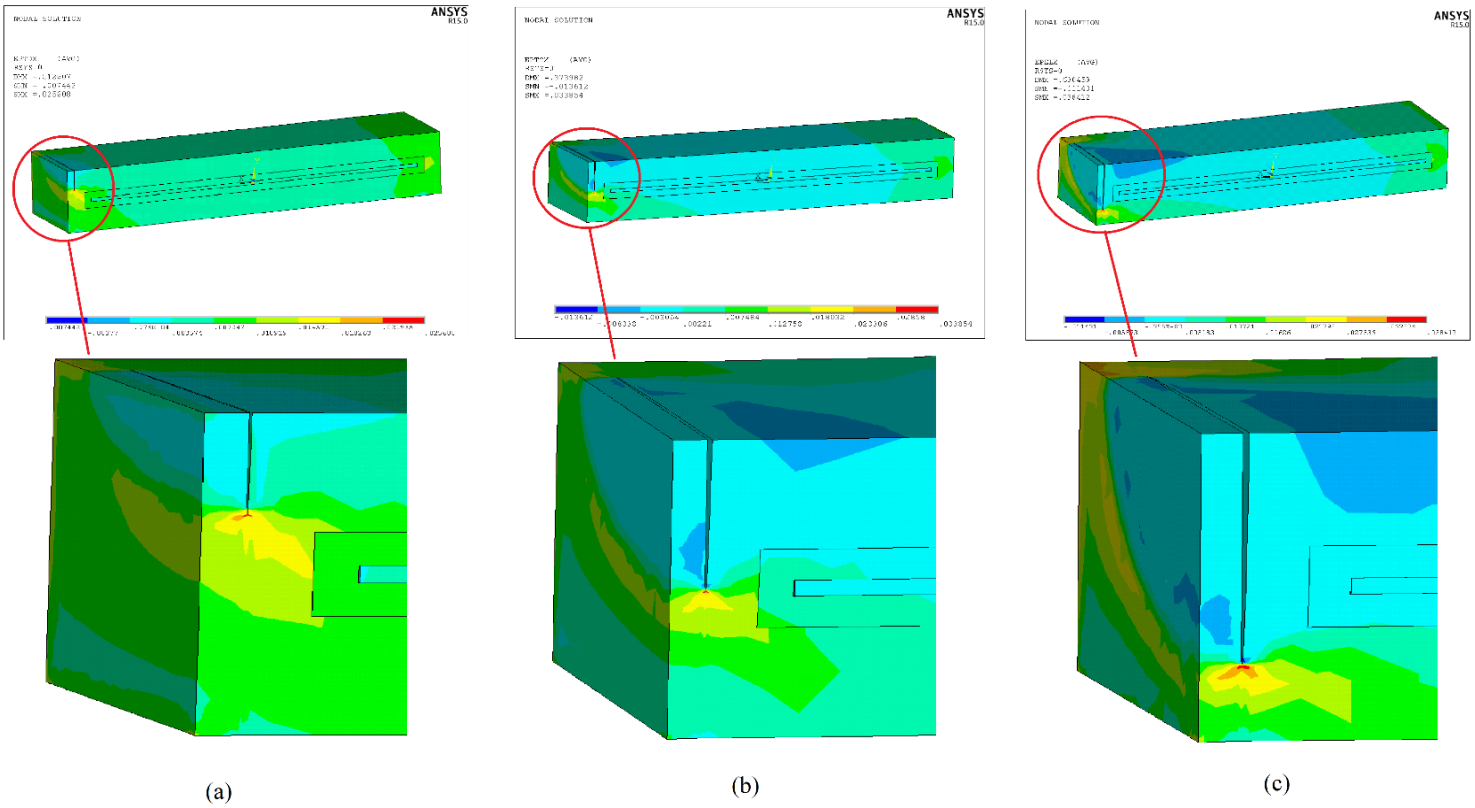

(a) (b) (c)

Fig. 7. Total Starin Contour/ Semi-elliptical crack propagation in Short RVE (a) a/w= 0.25 (b) a/w= 0.5 (c) a/w=0.7

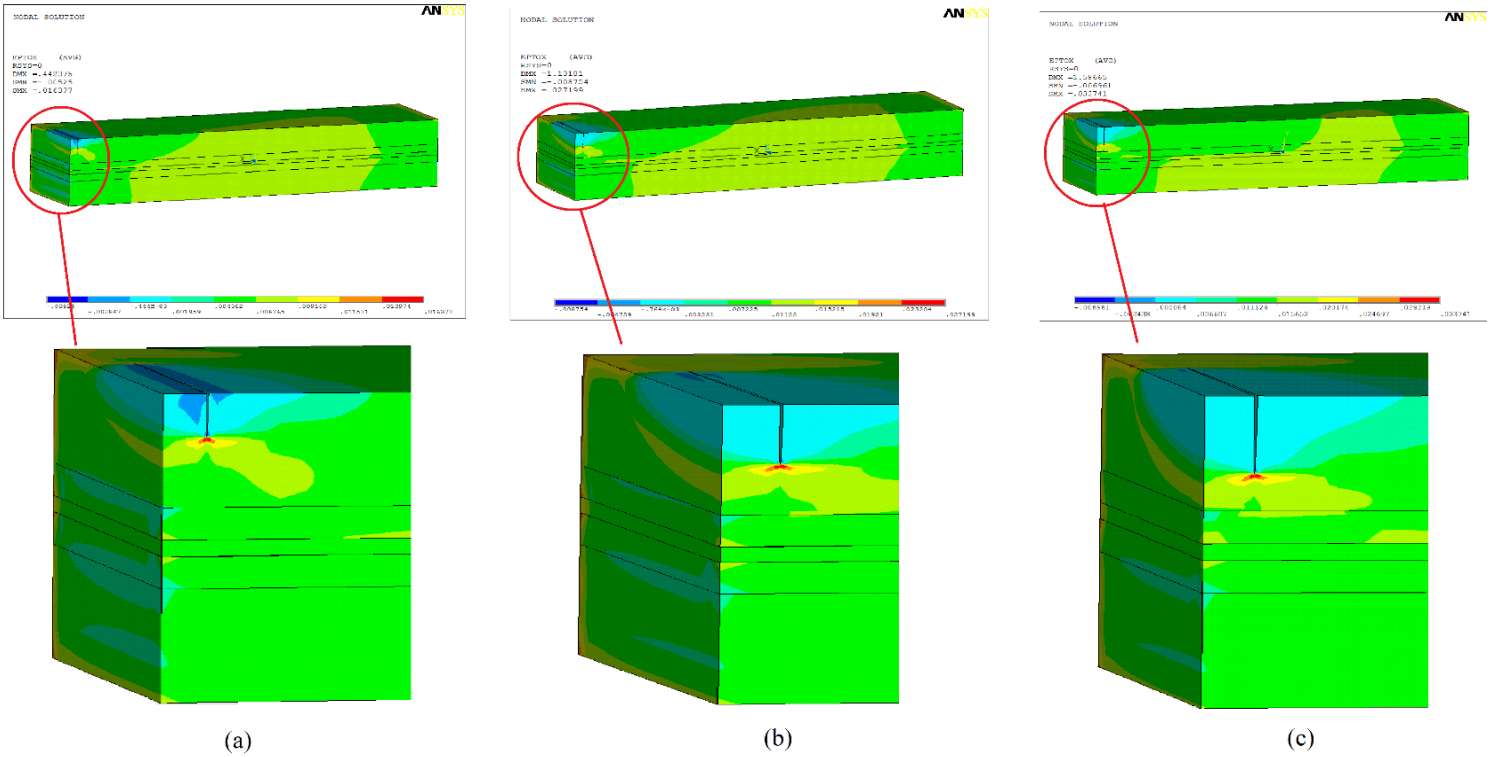

(a) (b) (c)

Fig. 8. Total Starin Contour/ Semi-elliptical crack propagation in Long RVE (a) a/w= 0.15 (b) a/w= 0.2 (c) a/w= 0.25

In accordance with the Fig.9, the total strain of short RVE is described, emphasizing the debonding damage between clay and interphase region as well as crack opening.

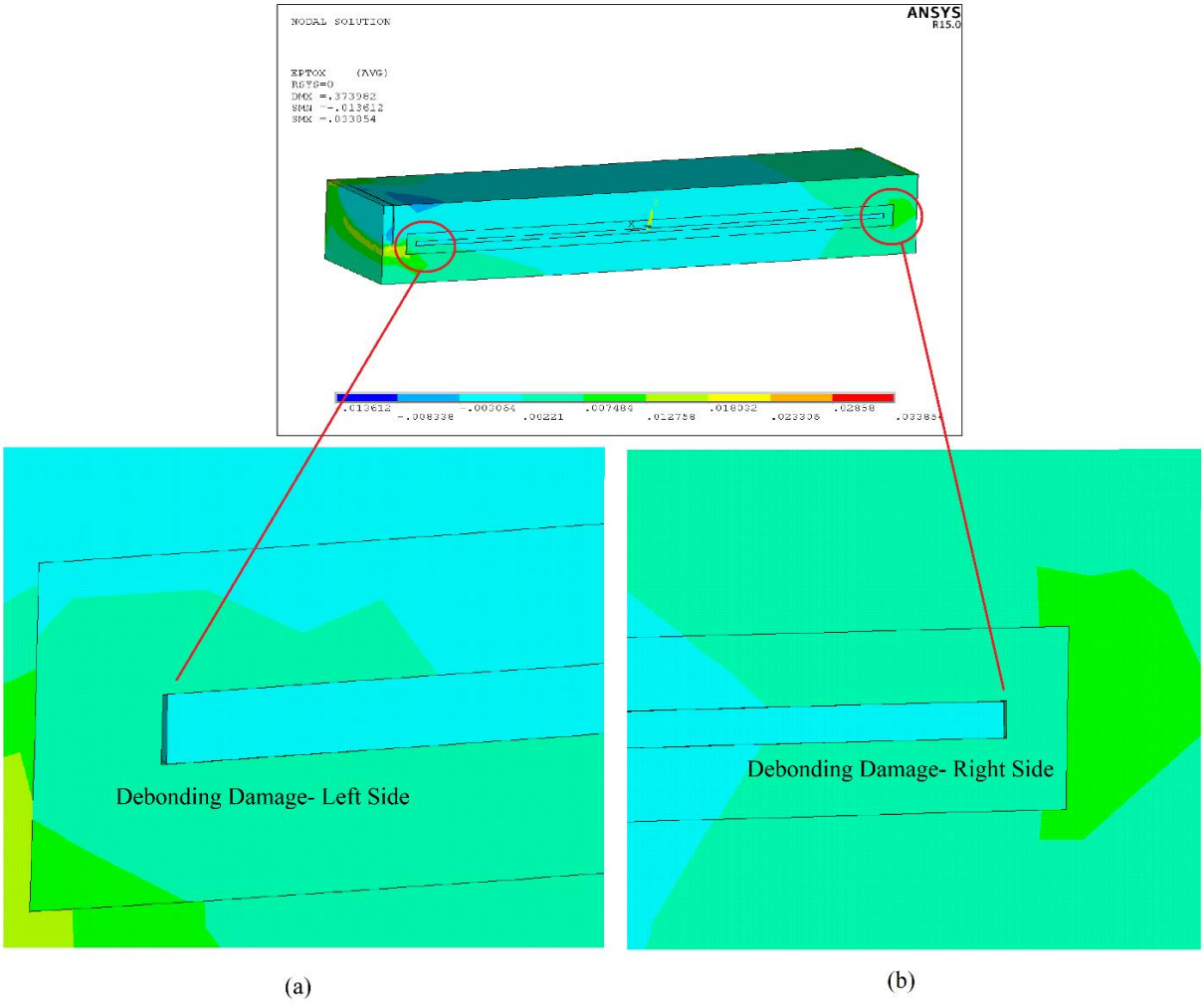

Fig. 9. Short RVE with CZM -Total elastic/plastic strain (a) Debonding damage left side (b) Right side

The dominant factors that have significant effects on J-integral at any point belonging to crack front are categorized as: crack dimensions (*a*, *c*), angular position of intended point on crack front (φ), crack location with respect to RVE's length (*l*), clay content percentage, RVE properties e.g. long/short type modeling, with and without CZM mode and interphase stiffness, which are elaborated subsequently. Figs. 10 and 11 exhibit the influence of crack dimensions on dimensionless energy release rate, J_0/J. The values of this ratio demonstrate the significant effect of nanoclay on the fracture behavior of neat epoxy even at the outermost points of crack front. It should be expressed that the horizontal and vertical axes imply the non-dimensional position

angle on crack front and normalized J integral, respectively. Normalizing factor (J_o) denotes the contour integral for a crack with the same size in neat epoxy without any inclusion. Moreover, it should be indicated that in the nanocomposite models, the interfacial enhancement index was adopted as 40. As shown in the Fig.10, normalized J increases during the crack propagates along its longer diameter *c*. In such 3D configuration, the middle region of crack front $\left(\frac{\pi}{4} < \varphi < \frac{3\pi}{4} approximately\right)$ in the vicinity of clay and interphase, is subjected to a high increase in normalized J rate than the other zones. Thus, it is worth noting that all contours achieved to their apexes at the deepest point ($\varphi = \pi/2$) which is in close proximity to the clay platelet.

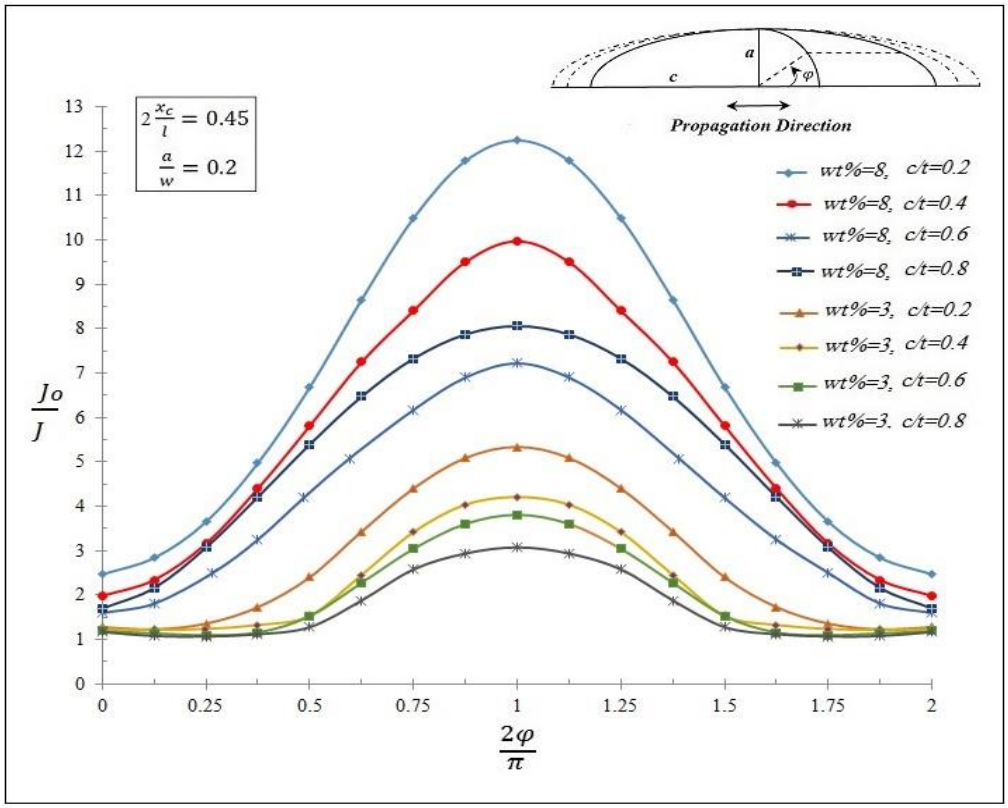

Fig. 10. Variation of normalized J along crack front for several crack sizes in the short RVE; propagation along Z direction

On the contrary, the tendency of crack propagation improves towards the end regions of crack ($\varphi = 0\ , \pi$) in 'c' direction. The impediment effect of nanoclay on crack propagation in 'a' direction (towards platelet thickness), is stronger than that of transverse direction (along 'c' diameter) on the crack edge. Furthermore, the amount of clay content has a remarkable influence on the crack characteristics. As a matter of fact, once local stiffness goes up, the crack tendency

to growth decreases. In accordance with Fig. 11, at crack endpoints $\left(0 < \varphi < \frac{\pi}{8},\ \frac{15\pi}{8} < \varphi < 2\pi\ approximately\right)$ by increasing clay content (%), J0/J decreases. This anomalous phenomenon is observed through 3D nature of existing model [59]. In a RVE with a higher percentage of nanoclay, J_0/J for deepest point is almost 5 times greater (at maximum condition) than crack endpoints. Therefore, by moving away from deepest point on the crack front of short RVE model, normalized energy reduces, owing to the decline in clay influence on crack characteristics. Comparing the crack propagation between Y and Z direction, the convexity of curves in-plane(XY) successive crack positions is more than to out-of-plane ones.

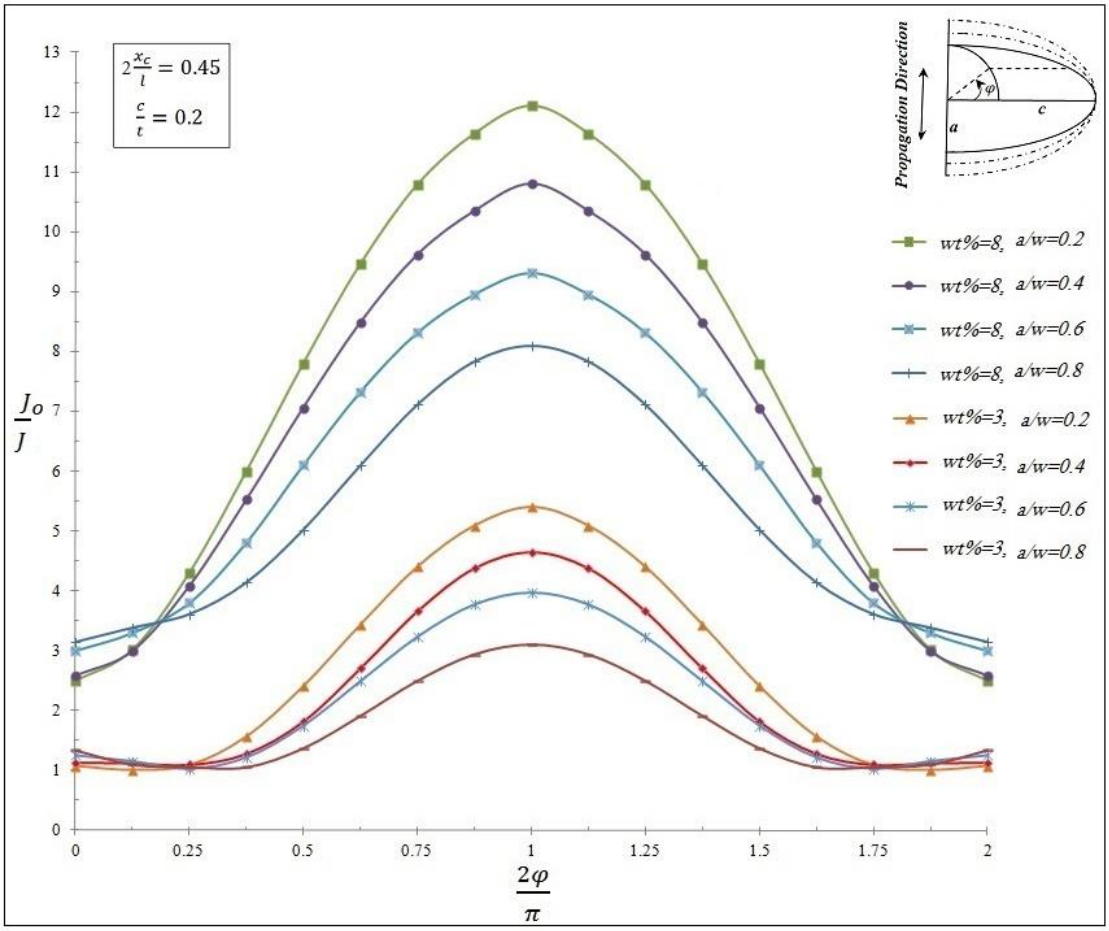

Fig. 11. Variation of normalized J along crack front for several crack sizes in the short RVE; propagation along Y direction

The variation trend in normalized J at the deepest point of crack front versus clay content considering various crack locations is depicted in Fig. 12. As previously mentioned, the inclusion volume fraction plays a significant role on toughening. It should be noted, *a* and *c* have been

chosen as one-fifth of *w* and t, respectively. Considering aforementioned crack size, there is a continuous enhancement in dimensionless J as the value of clay content increases. However, this noticeable improvement observed by increasing clay volume fraction up to about 8%, is at least 4 times in comparison with the lowest clay content.

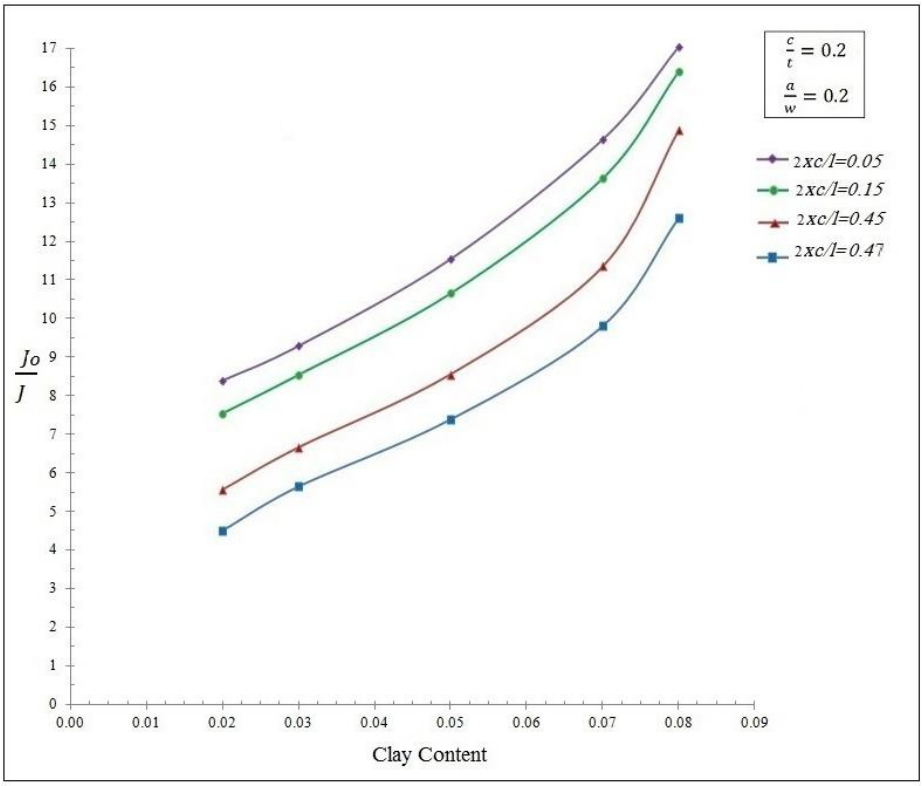

Fig. 12. Variation of normalized J versus clay content at different crack locations the in the short RVE

In order to evaluate the effect of crack location on contour integrals, twelve positions are defined and their corresponding results are reflected in Fig. 13 along the crack front. Significant observed drop in normalized J factor is attributed to dwindling effect of nanoclay presence on crack driving force at the end of RVE since toughening factor of nanocomposite diminishes with a high gradient in the region which is far from nanoclay ($2x_c/l$ = 1). Adversely, crack propagation is highly hindered when the crack is located at the mid-plane of short RVE model ($2x_c/l$ = 0). It is worthwhile to indicate that, in the nanocomposite model with higher clay contents, the influence of crack position is more tangible than the model with lower inclusion contents. As described in the Fig.13, due to the three dimensional clay geometry which embedded in epoxy, the normalized J at crack end points (θ= 0, π) approximately dropped by 20% more than the deepest

point($\varphi = \pi/2$) in clay content of 8 wt%. Unequivocally, this result is inferred from the presence of nanoclay which is thoroughly embedded in the surrounding matrix.

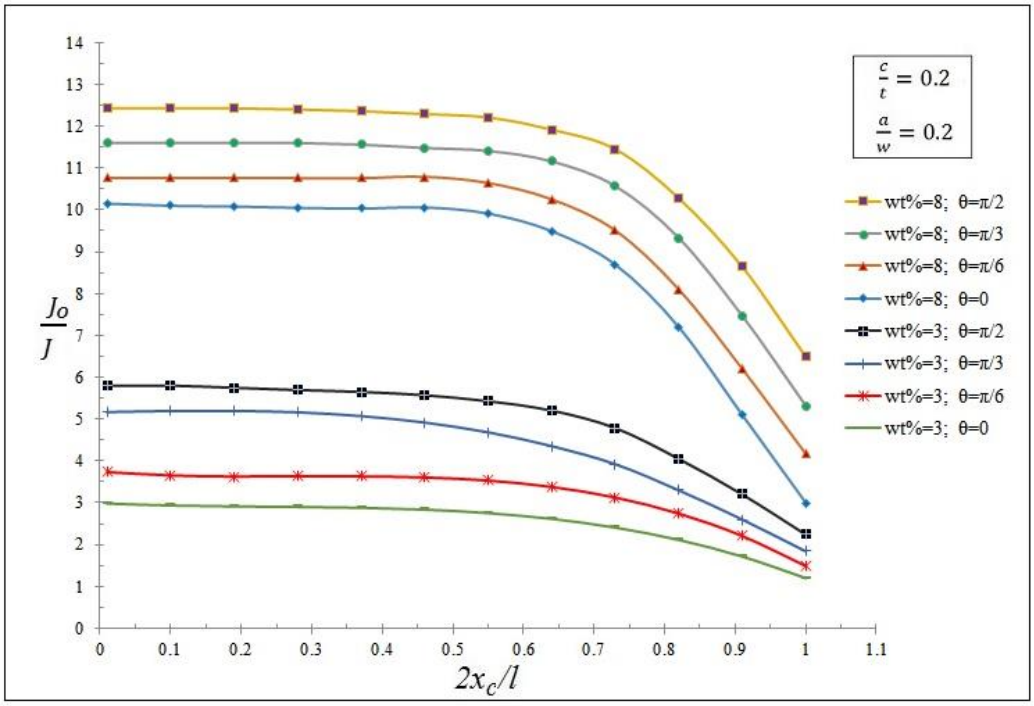

Fig. 13. J_o /J versus longitudinal crack positions for several points along the crack front in the short RVE

As depicted in Fig. 14, the influence of CZM on dimensionless energy release rate is scrutinized for both long and short RVE models. It is evident from the graph that incorporating CZM between clay and interphase decreases the elastic modulus of nanocomposite leading to an increase in the normalized J. In the short RVE model, the maximum value of J_0/J taking place at the deepest point of semi-elliptical crack decreases about 26% in 8 wt% of clay content in the model possessing CZM compared to the short model without CZM. By reducing the percentage of clay contents, the obvious effect of CZM on energy release rate diminishes. For instance, in 3% of clay content, exploiting of CZM results in 18% reduction in J_0/J.

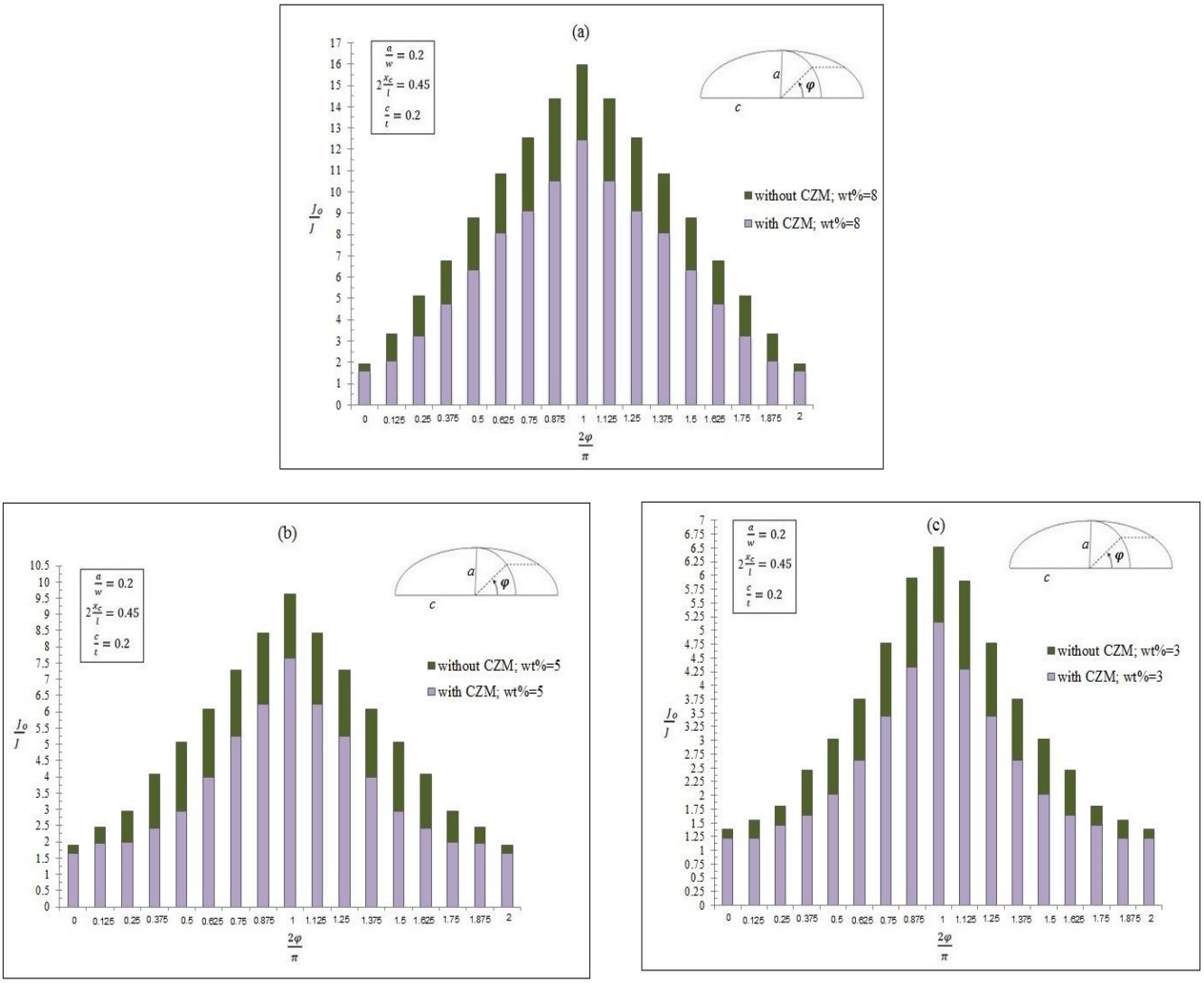

Fig. 14. Influence of CZM on normalized J along crack front in the short RVE: (a) wt=8%, (b) wt=5%, (c) wt=3%

Recalling from previous section, the type of load transferring to clay has an undeniable influence on the mechanical behavior of RVE. Indeed, in the long type model, load is directly transferred to inclusion and as a consequence of this modeling approach, the elastic modulus of such RVE is considerably higher than short RVE model. In contrast, in the latter, load is transferred from clay through the medium via non-perfect bonding and the main outcome of such modeling approach is lower stiffness which is consistent with published experimental data. The influence of long/short type RVE on crack toughening factor is demonstrated in Fig. 15. As it can be seen, RVE selection strategy can intensify the crack energetic; long type RVE results in the

amplification of Jo/J up to about 35% in comparison with the short one at $\varphi = \pi/2$. The most affected zones belong to crack deepest point indicating the significant effect of load transfer type on local stiffness in vicinity of clay platelet.

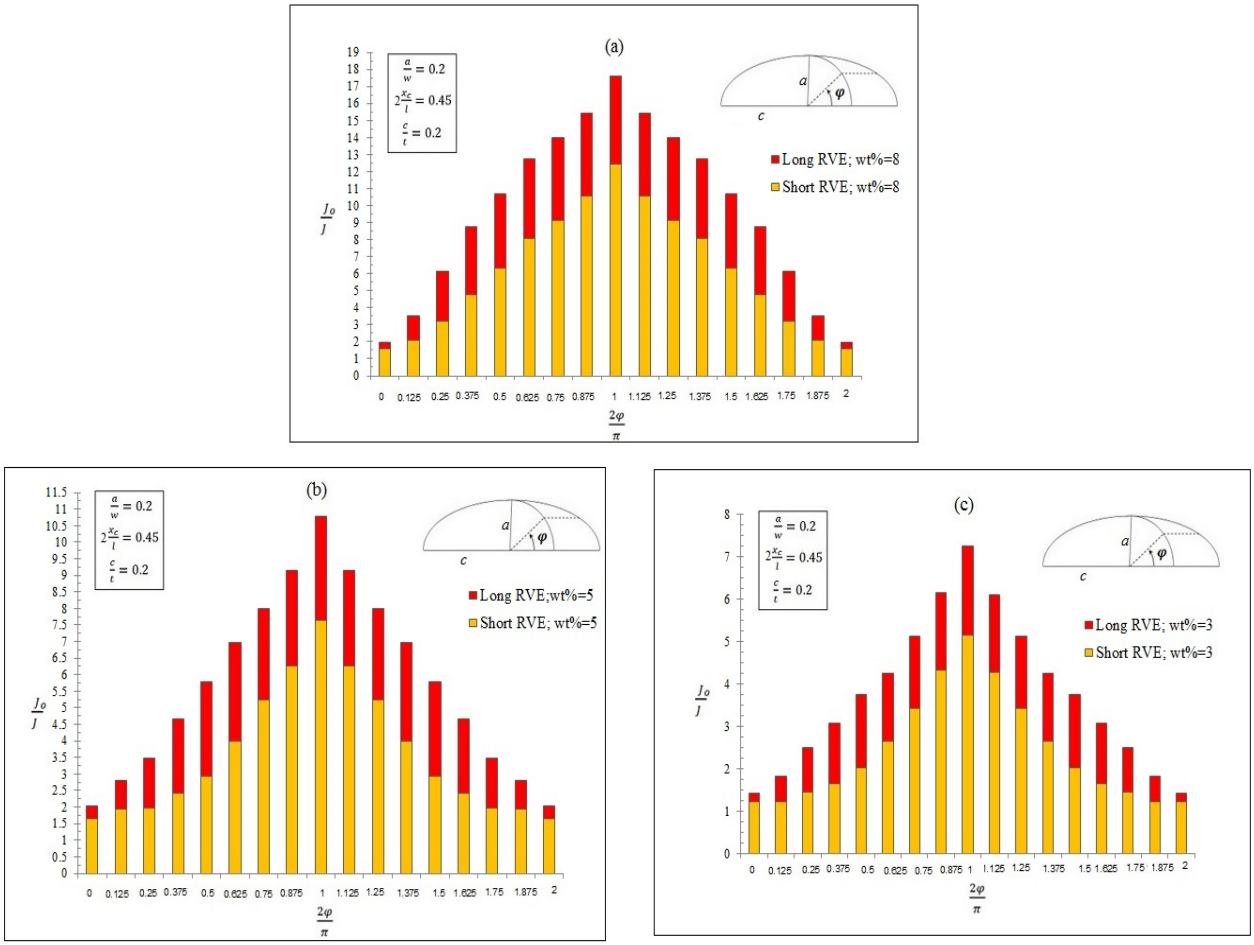

Fig. 15. Influence of long/short RVE type on normalized J along crack front in: (a) wt=8%, (b) wt=5%, (c) wt=3%

Thanks to the remarkable influence of interfacial enhancement index on interphase elastic moduli, IEI variation effect on the crack behavior should also be investigated. The variation of normalized J versus interphase thickness in different n values at the deepest crack tip is shown in Fig. 16. The normalizing factor utilized herein, is J computed with n=40. Remarkably, the magnitude of dimensionless J is augmented by decreasing of IEI. Furthermore, for higher amounts of IEI than selected IEI (n=40), as interphase thickness increases, J_n diminishes. On

contrary, by decreasing IEI (lower than n=40), non-dimensional factor (J_n/ J_{40}) becomes smaller than unit because of elastic modulus increment emanating from lower IEI values.

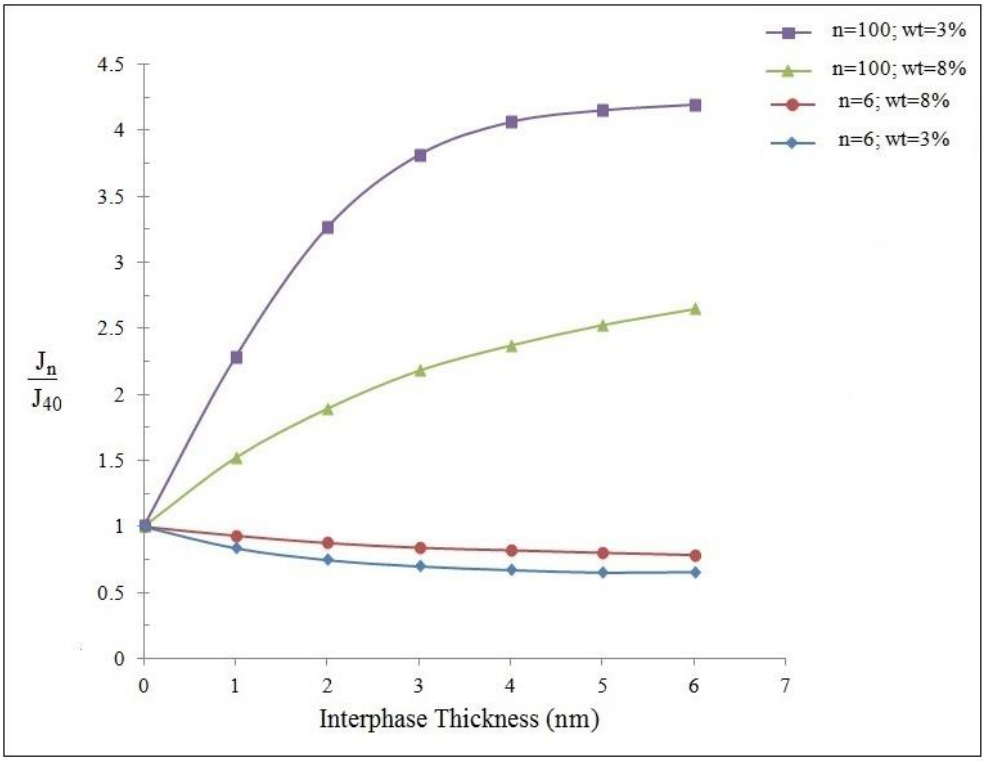

Fig. 16. **N**ormalized J_n versus interphase thickness with respect to different interfacial enhancement indices

3. Conclusion

The present work is devoted to investigate the role of non-bonded interaction between clay and polymer on fracture behavior of nanoclay reinforced polymers. For this purpose, a 3-D multi-scale FE model is constructed. Normalized J contour integral is defined and computed as a toughening criterion for monitoring the influence of crack existence and its characteristics. The variation of this factor as a function of crack geometry, crack location and RVE aspects such as clay debonding damage are examined thoroughly. The mix-mode CZM model is implemented accounting for non-perfect bonding between clay and epoxy. The results reveal the pronounced effect of clay debonding on crack behavior which leads to local stiffness reduction. Likewise, the influence of interphase thickness on crack energetic pertaining to 3D crack front is studied and the results of which disclose that the deepest crack point is subject to higher toughening effects

in presence of nanoclay. The outcomes, furthermore, disclose that nanocomposite modeling strategy encompassing long/ short model and with /without CZM plays a critical role in toughening factor and therefore should not be neglected in numerical investigations. The remarkable results are listed as following:

- The crucial role of considering interface region and clay debonding on crack behavior
- The considerable effect of interphase thickness on crack behavior
- The remarkable difference of crack properties between 'Short RVE' and 'Long RVE' models
- The noticeable improvement of toughening factor in clay/epoxy nanocomposite than neat resin, in presence of non-bonding interaction between clay and surrounding matrix

References

1. Park JH, Jana SC. The relationship between nano- and micro-structures and mechanical properties in PMMA–epoxy–nanoclay composite. Polymer 2003; 44(7):2091–100.

2. Zhou Y, Pervin F, Biswas MA, Rangari VK, Jeelani S. Fabrication and characterization of montmorillonite clay-filled SC-15 epoxy. Mater Lett 2006; 60(7):869–73.

3. Ahmadi SJ, Huang YD, Li W. Review, synthesis routes, properties and future application of polymer-layered silicate nanocomposites. J Mater Sci 2004; 39:1919–25.

4. Maleki Moghadam R, Hosseini SA, Salehi M. The influence of Stone–Thrower–Wales defect on vibrational characteristics of single-walled carbon nanotubes incorporating Timoshenko beam element. Physica E 2014; 62:80–89.

5. Saber-Samandari S, Afaghi-Khatibi A, Basic D. An experimental study on clay-epoxy nanocomposites produced in a centrifuge. Composites Part B 2007; 38(1):102-107.

6. Hosseini SA, Saber-Samandari S, Maleki Moghadam R. Multiscale modeling of interface debonding effect on mechanical properties of nanocomposites. Polym Compos 2015. http://dx.doi.org/10.1002/pc.23639.

7. Roham Rafiee, Reza Maleki Moghadam, On the modeling of carbon nanotubes: A critical review, Composites: Part B 56 (2014)435–449.

8. Lauke B. Determination of adhesion strength between a coated particle and polymer matrix. Compos Sci Technol 2006; 66:3153-3160.

9. Lauke B. On the effect of particle size on fracture toughness of polymer composites. Compos Sci Technol 2008; 68:3365-72.

10. Zappalorto M, Salviato M, Quaresimin M. Influence of the interphase zone on the nanoparticle debonding stress. Compos Sci Technol 2011; 72:49-55.

11. Zappalorto M, Salviato M, Quaresimin M. A multiscale model to describe nanocomposite fracture toughness enhancement by the plastic yielding of nanovoids. Compos Sci Technol 2012;72; 1683-1691.

12. H.W. Wanga, H.W. Zhou, R.D. Peng, Leon Mishnaevsky Jr, Nanoreinforced polymer composites: 3D FEM modeling with effective interface concept, Compos Sci Technol 2011; 71: 980–988.

13. Vu-Bac N, Silani M, Lahmer T, Zhuang X, Rabczuk T. A unified framework for stochastic predictions of Young's modulus of clay/epoxy nanocomposites (PCNs). Comput Mater Sci 2015; 96: 520 – 535.

14. Silani M, Talebi H, Ziaei-Rad S, Kerfriden P, Bordas S, Rabczuk T. Stochastic Modelling of Clay/Epoxy Nanocomposites. Compos Struct 2014; 118: 241-249.

15. Heydari-Meybodi M, Saber-Samandari S, Sadighi M. A new approach for prediction of elastic modulus of polymer/nanoclay composites by considering interfacial debonding: Experimental and numerical investigations. Compos Sci Technol 2015; 117: 379-385.

16. Wang B, Qi N, Gong W, Li XW, Zhen YP. Study of microstructure and mechanical properties for epoxy resin/montmorillonite nanocomposites by positron. Radiat Phys Chem 2007; 76:146–9.

17. Wang L, Wang K, Chen L, Zhang Y, He C. Preparation, morphology and thermal/mechanical properties of epoxy/nanoclay composite. Composites Part A 2006; 37: 1890–1896.

18. Shi HZ, Lan T, Pinnavaia TJ. Interfacial effects on the reinforcement properties of polymer–organoclay nanocomposites. Chem Mater 1996; 8:1584–7.

19. Rafiee R, Shahzadi R. Mechanical Properties of Nanoclay and Nanoclay Reinforced Polymers: A Review. Polym. Compos. 2018, DOI 10.1002/pc.24725.

20. Boo WJ, Sun L, Liu J, Moghbelli E, Clearfield A, Sue HJ, Pham H, Verghese N. Effect of nanoplatelet dispersion on mechanical behaviour of polymer nanocomposites. J. Polym. Sci., Part B: Polym. Phys. 2007; 45:1459–69.

21. Tjong SC, Bao SP. Fracture toughness of high density polyethylene/SEBS-g-MA/montmorillonite nanocomposites. Compos Sci Technol 2007;67(2):314-323.

22. Lim SH, Dasari A, Yu ZZ, Mai YW, Liu S, Yong MS. Fracture toughness of nylon 6/organoclay/elastomer nanocomposites. Compos Sci Technol 2007;67(14): 2914–2923.

23. Zappalorto M, Salviato M, Quaresimin M. Mixed mode (I + II) fracture toughness of polymer nanoclay nanocomposites. Eng Fract Mech 2013; 111:50-64.

24. Wang K, Chen L, Wu J, Toh ML, He C, Yee AF. Epoxy Nanocomposites with Highly Exfoliated Clay: Mechanical Properties and Fracture Mechanisms. Macromolecules 2005; 38: 788-800.

25. Saminathan K, Selvakumar P, Bhatnagar. N Fracture studies of polypropylene/nanoclay composite. Part I: Effect of loading rates on essential work of fracture. Polym Test 2008;27(3): 296–307.

26. Saminathan K, Selvakumar P, Bhatnagar N. Fracture studies of polypropylene/nanoclay composite. Part II: Failure mechanism under fracture loads. Polym Test 2008;27(4):453–458.

27. Rostamiyan Y, Fereidoon AB, Hamed Mashhadzadeh A, Khalili MA. Augmenting epoxy toughness by combination of both thermoplastic and nanolayered materials and using artificial intelligence techniques for modeling and optimization. J Polym Res 2013; 20:135, DOI 10.1007/s10965-013-0135-3.

28. Maleki Moghadam R, Saber-Samandari S, Hosseini SA. On the tensile behavior of clay-epoxy nanocomposite considering interphase debonding damage via mixed-mode cohesive zone material. Composites Part B 2016; 89:303-315.

29. Venkatesh GS, Deb A, Karmarkar A. Characterization and finite element modeling of montmorillonite/polypropylene nanocomposites. Mater Des 2012; 35: 425–433.

30. Figiel L. Effect of the interphase on large deformation behaviour of polymer–clay nanocomposites near the glass transition: 2D RVE computational modeling. Comput Mater Sci 2014; 84:44–254.

31. Pisano C, Figiel L. Modelling of morphology evolution and macroscopic behavior of intercalated PET–clay nanocomposites during semi-solid state processing. Compos Sci Technol 2013; 75: 35–41.

32. Silani M, Ziaei-Rad S, Esfahanian M, Tan VBC. On the experimental and numerical investigation of clay/epoxy nanocomposites. Compos Struct 2012; 94: 3142–3148.

33. Dai G, Mishnaevsky Jr L. Damage evolution in nanoclay-reinforced polymers: A three-dimensional computational study. Compos Sci Technol 2013; 74:67–77.

34. Silani M, Ziaei-Rad S, Talebi H, Rabczuk T. A Semi-Concurrent Multiscale Approach for Modeling Damage in Nanocomposites. Theor Appl Fract Mec 2014; 74: 30-38.

35. Msekh MA, Cuong N.H, Zi G, Areias P, Zhuang X, Rabczuk T. Fracture properties prediction of clay/epoxy nanocomposites with interphase zones using a phase field model. Eng Fract Mech 2018; 188:287-299.

36. Msekh MA, Silani M, Jamshidian M, Areias P, Zhuang X, Zi G, He P, Rabczuk T. Predictions of J integral and tensile strength of clay/epoxy nanocomposites material using phase field model. Composites Part B 2016; 93: 97-114.

37. Larson MC. Experimental and computational models for three-dimensional crack–fiber interactions. Exp Mech 1997; 37(4):445–51.

38. Lee HK, Ju JW. A three-dimensional stress analysis of a penny-shaped crack interacting with a spherical inclusion. Int J Damage Mech 2007; 16:331–59.

39. Hadi A, Weichert D. Three-dimensional interaction between a crack front and particles. Int J Numer Methods Eng 1998; 42:1463–76.

40. JI XL, Jing JK, Jiang W, Jiang BZ. Tensile modulus of polymer nanocomposites. Polym Eng Sci 2002; 42: 983-993.

41. Luo JJ, Daniel IM, Characterization and Modeling of Mechanical Behavior of Polymer/Clay Nanocomposites. Compos Sci Technol 2003; 63: 1607-1616.

42. Wang J, Pyrz R. A Prediction of the overall moduli of layered silicate-reinforced nanocomposites — Part I: basic theory and formulas. Compos. Sci. Technol 2004; 64: 925–934.

43. Saber-Samandari S, Afaghi-Khatibi A. The effect of interphase on the elastic modulus of polymer based nanocomposites. Key Engineering Material 2006; 312: 199-204.

44. Saber-Samandari S, Afaghi-Khatibi A. Evaluation of Elastic Modulusof Polymer matrix Nanocomposites. Polymer Composites 2007, DOI 10.1002/pc.20322.

45. Pahlavanpour M, Moussaddy H, Ghossein E, Hubert P, Lévesque M. Prediction of elastic properties in polymer–clay nanocomposites: Analytical homogenization methods and 3D finite element modeling. Comput Mater Sci 2013; 79: 206–215.

46. Manevitch OL, Rutledge G. Elastic properties of a single lamella of montmorillonite by molecular dynamics simulation. J Phys Chem B 2004; 108:1428–35.

47. Chen B, Evans JRG. Elastic moduli of clay platelets. Scripta Materialia 2006; 54:1581–1585.

48. ANSYS Inc. Theory manual. SAS IP Inc. 2012. Release 14.5.

49. Chen Y, Chia JYH, Su ZC, Tay TE, Tan VBC. Mechanical characterization of interfaces in epoxy-clay nanocomposites by molecular simulations. Polymer 2013; 54: 766-773.

50. Rafiee R, Shahzadi R. Predicting mechanical properties of nanoclay/polymer composites using stochastic approach. Composites Part B 2018; 152: 31-42.

51. Alfano G, Crisfield MA. Finite Element Interface Models for the Delamination Anaylsis of Laminated Composites: Mechanical and Computational Issues. Int J Numer Methods Eng 2001; 50: 1701-1736.

52. ANDERSON TL. Fracture Mechanics: Fundamentals and Applications, Third Edition. CRC, 2004.

53. Ferreira JAM, Borrego LP, Costa JDM, Capela C. Fatigue behaviour of nanoclay reinforced epoxy resin composites. Composites Part B 2013; 52:286–291.

54. Saxena A. Nonlinear Fracture Mechanics, CRC, 1998.

55. Claudio RA, Baptista R, Infante V, Branco CM. Life Prediction Using Finite Elements in Complex Geometries. Jornadas De Fractura 2002; 8: 201-222.

56. Shahani AR, Habibi SE. Stress intensity factors in a hollow cylinder containing a Circumferential semi–elliptical crack subjected to combined loading. Int. J. Fatigue 2007; 29(1):127-140.

57. Broek D. The Practical Use of Fracture Mechanics. Kluwer Academic Publishers Galena OH,1998.

58. Sheng N, Boyce MC, Parks DM, Rutledge GC, Abes JI, Cohen RE. Multiscale micromechanical modeling of polymer/clay nanocomposites and the effective clay particle. Polymer 2004; 45: 487–506.

59. A.A. Gawandi, J.M. Whitney, G.P. Tandon c R.B. Brockman, Three-dimensional analysis of the interaction between a matrix crack and nanofiber, Composites: Part B 40 (2009) 698–704